

Kinetics modeling of water sorption and nutrient release of hydroxypropyl cellulose/carboxymethyl cellulose/sodium alginate hydrogel blends for agricultural applications

Paul Jake Nalzar^{1*} , Terence Tumolva¹ 

¹ Department of Chemical Engineering, University of the Philippines, Quezon City, Philippines

* Corresponding author's e-mail: pbnalzar@up.edu.ph

ABSTRACT

This study aimed to mathematically define the water sorption and nutrient release of HPC/CMC/Alg agricultural hydrogels by determining the kinetic parameters for models under more realistic mechanisms such as (i) concentration-dependent diffusion coefficients and (ii) moving boundary. The Berens-Hopfenberg model was modified to account for the concentration-dependence of diffusion coefficients. The water sorption behavior resulted in a high correlation with a diffusion-fraction $x_F = 0.3086$, diffusion coefficient at infinite dilution per squared radius $D_0' = 0.00000981 \text{ min}^{-1}$, and concentration coefficient $\beta = 0.1632$. The behavior of nutrient release resulted in a high correlation with $x_F = 0.2398$, $D_0' = 0.05976 \text{ min}^{-1}$, and $\beta = 0.9205$. With low values of x_F , both behaviors exhibited uptake that are more significant during relaxation than diffusion. To account for moving boundaries due to water sorption, a semi-empirical model was derived based on Fick's Law. The water sorption behavior resulted in a high correlation with diffusion coefficient $D = 0.0199 \text{ mm}^2/\text{min}$, correction factor $A = 1.291$, and time coefficient $K = 0.0342$. The nutrient release achieved a high correlation with $D = 0.272 \text{ mm}^2/\text{min}$, $A = 1.530$, and $K = 0.203$. When applied to second-cycle water sorption data, the fitted models were found to be overestimated. This is due to the permanent changes in the structure of the polymer matrix during swelling-deswelling.

Keywords: hydrogels, diffusion, moving boundary, mass transfer.

INTRODUCTION

The Philippine agriculture sector has continued to experience a significant decline in the country's total GDP contribution, from 10% in 2022 to 8% in 2024 (Philippine Statistics Authority, 2024). This is caused by inefficient and insufficient irrigation systems, lack of machinery, and underutilization of fertilizers. Innovative solutions such as cloud seeding, shelterbelts, and even utilization of drought-tolerant crops are financially challenging and difficult to implement (Garduque et al., 2020). Moreover, only 57% of the nutrients in the fertilizer applied is taken up by plants; the excess 43% leaches, thereby causing environmental degradation through depletion of soil nutrients and run-off to nearby bodies of water (Magcale-Macandog et al., 2016).

A solution to address water shortage and fertilizer underutilization is the use of hydrogels as

water and nutrient carrier. Hydrogels are water-swollen polymeric materials that maintain a three-dimensional structure (Rizwan et al., 2024). They have recently emerged in the field of agriculture due to their superabsorbent properties demonstrated by high water holding capacity and soil moisture retention, as well as controlled solute release properties (Saruchi et al., 2019). However, most commercially available hydrogels are made of polyacrylate and acrylate derivatives which are synthetic, non-renewable, and toxic to the environment (Lin et al., 2024; Zhang et al., 2025). Hence, natural and renewable sources can be used as alternatives to these synthetic polymers.

Garduque et al. (2020) synthesized a hydrogel blend of hydroxypropyl cellulose (HPC), carboxymethyl cellulose (CMC), and alginate. HPC is often a good candidate in hydrogel synthesis due to the hydrogen bonding provided by

its hydroxyl groups (Nalzaró et al., 2019; Zhang et al., 2024). CMC is a smart cellulose derivative as it is sensitive to changes in ionic strength (Akalın and Pulat, 2018). Meanwhile, alginate is the component that causes to form a gel under controlled proportions of cations via ionic gelation (Yetilmezsoy et al., 2024). Garduque et al. (2020) identified that 42% HPC, 29% CMC, and 29% alginate is the optimal blend upon conducting an optimization via weighted averaging based on the water sorption and nutrient loading capacities.

Andes et al. (2021) improved this finding by doing performance testing and investigating the reusability of the synthesized hydrogels in Figure 1. They found out that the swelling ratio gradually decreases after multiple cycles of swelling-deswelling and that the behavior of the nutrient release consists of an initial fast-release response followed by an equilibrium release. However, none of these findings provide insight on how the internal structure of the hydrogels react to the stresses brought about by water sorption, how fast this mechanism proceeds, nor what factors affect these reactions. Hence, there is a need to mathematically model its behavior to predict the performance of hydrogels without having to perform additional experiments

The main objective of this research is to complement the study of Andes et al. (2021) by mathematically defining the kinetics behavior of water sorption and nutrient release of the nutrient-loaded HPC/CMC/Alg hydrogels under more realistic mechanisms. Specifically, the research aims to determine the kinetic parameters of a concentration-dependent water sorption and nutrient release of the hydrogels using several models and to predict their performance using the determined parameters. The mathematical modeling aspect in this research will test established models enumerated in the succeeding section. A semi-empirical model

will also be developed and tested in this study and it will be derived in the succeeding sections.

This study will focus on the kinetics modeling of the water sorption and nutrient release behavior of the HPC/CMC/Alg hydrogels using the optimal blend determined by Garduque et al. (2020). The water sorption and nutrient release data of Andes et al. (2021) will be utilized in the mathematical modeling. Power law model will be used as a preliminary model to compare the succeeding predictive models with. Nutrient release studies will lump the fertilizer nutrients as one entity, and not separately as nitrogen, phosphorus, and potassium.

MATHEMATICAL MODELS

The swelling behavior of hydrogels can be categorized into three steps. First, water molecules attach into the polar functional groups of the polymeric network like hydroxyl groups and carboxyl groups (Casalme et al., 2016). Next, polymer chains untangle and transition into a glassy state in a manner of relaxation, thereby providing more space for water molecules to attach. Lastly, the polymeric network continues to expand as more water enters until saturation. At saturation, the forces of osmotic pressure and elastic binding balance each other (Fei et al., 2024) This depiction of hydrogel swelling is proven to be true regardless of whether the hydrogel is homogeneous or heterogeneous. Homogeneous hydrogels are those that are made of only one polymeric material. On the other hand, heterogeneous hydrogels are made of more than one polymeric material, which are common for applications that not one material can address as in the case of the individual reinforcements of HPC, CMC, and alginate by Garduque, et al. (2020).

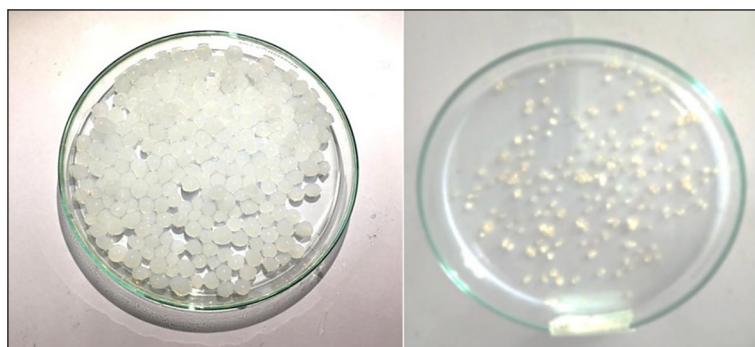


Figure 1. Synthesized HPC/CMC/Alg hydrogels: (a) before drying, (b) after drying (Andes et al., 2021)

During the transition between glassy state and rubbery state, a coupling between mechanical stress and diffusion is observed. As shown in Figure 2, swellable polymers like hydrogels exhibit stress relaxation when stretched due to water uptake. When this constant strain brought is induced, the polymer matrix slowly re-swells to an equilibrium volume by rearranging its initial polymeric structure as physical bonds rupture (Giustiniani et al., 2023; Takigawa et al., 2002). The penetration of moisture during the preceding swelling mechanism results to a reduction of interstitial suction pressure within the hydrogel but an increase in the elastic stress, signifying that this subsequent stage is characterized as viscoelastic in nature (Chiarelli et al., 1993; Yang et al., 2021). Swelling also results in a redistribution of the polymeric chains while the amount of these chains in the medium remains unchanged. Increased moisture content in water sorption studies can be linked to an increase in porosity when a polymeric material swells (Nicasy et al., 2024).

The Fick’s laws of diffusion are used in modelling the transport kinetics of the swelling phenomenon in these swellable hydrogels. Fick’s second law of diffusion, shown in Eq. 1, is used to quantitatively describe the relation between time and concentration of molecules in the network of spherical hydrogels. Common applications of Fick’s second law include modelling the controlled drug release in pharmaceutical and biomedical applications of hydrogels (Nguyen et al., 2024; Qureshi et al., 2023).

$$\frac{\partial p}{\partial t} = D \frac{\partial^2 p}{\partial r^2} \tag{1}$$

where: p – mass concentration, t – time, D – diffusion coefficient, r – radial position

From Fick’s second law of diffusion in Equation 1, different models have been developed

according to mechanism. These models include the commonly used Korsmeyer-Peppas and Berens-Hopfenberg models and the modified models accounting for non-idealities such as concentration-dependent diffusion coefficients and diffusion with moving boundaries. The water sorption data and nutrient release data of this research will be fitted into these models. The goal of data fitting is to determine the values of the kinetic parameters present in these various models that can best represent the sets of experimental data points. Data fitting is often done by minimizing the differences between the model’s predicted values and the actual data.

Model for diffusion mechanism

Ritger and Peppas (1987) explored the applicability of the power law expression to the diffusion behavior of hydrogels where M_t is the amount of solute that had diffused at any given time t while M_∞ is the total amount of solute that had diffused (i.e., amount at hydrogel saturation). This was the basis of the commonly known Korsmeyer-Peppas model in Equation 2 which involves linearization techniques. By solving Fick’s first and second laws of diffusion for different geometries and truncating some terms for the sum of errors to simplify the formulas, they reported that the power law expression fits only the first 60% uptake of the process (Korsmeyer et al., 1983).

$$\frac{M_t}{M_\infty} = kt^n \tag{2}$$

where: M_t – mass of solute that had diffused at any given time t , M_∞ – mass at hydrogel saturation, k – diffusion constant, n – diffusion exponent

Figure 3 shows the typical diffusion mechanism of water sorption into the hydrogel matrix.

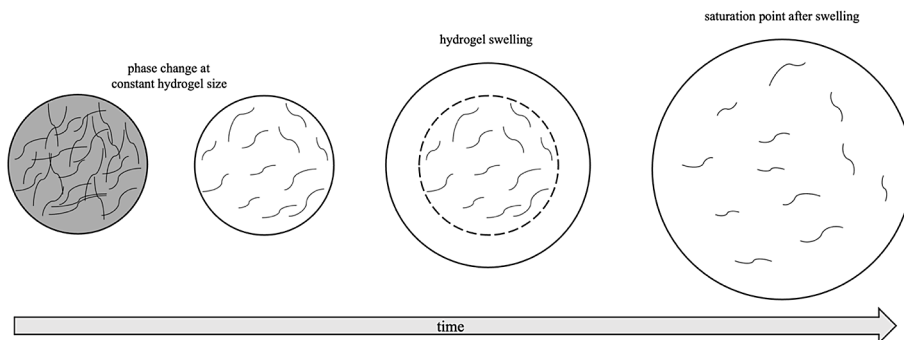


Figure 2. Sorption phenomena of swellable hydrogels

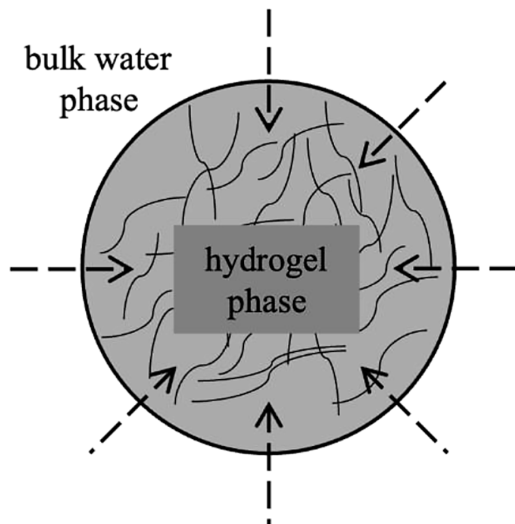


Figure 3. Diffusion mechanism of swelling

The diffusion constant k accounts for the geometry and the physical properties of a sample, while the diffusion exponent n describes the manner of swelling which is summarized in Table 1. This model was used by Boztepe et al. (2015) to model the swelling of acrylamide-based hydrogels by intelligent systems and found out that k is dependent on the crosslinker concentration. It is also applicable to several geometries as is the case of Fosca et al. (2022) where cylindrical

Table 1. Type of transport dictated by the diffusional exponent (Korsmeyer et al., 1983)

Diffusion exponent, n	Type of transport
$n < 0.5$	Pseudo Fickian
$n = 0.5$	Case I (Fickian)
$0.5 < n < 1.0$	Anomalous non-Fickian
$n = 1.0$	Case II (non-Fickian)
$n > 1.0$	Superanomalous non-Fickian

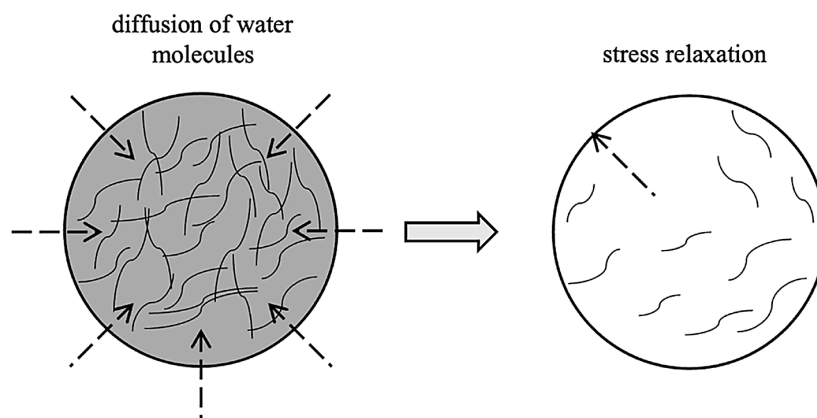


Figure 4. Diffusion-relaxation mechanism of swelling

samples of calcium phosphate cements or CPCs are used as drug delivery carriers for bone healing and regeneration.

Model for diffusion-relaxation mechanism

Berens and Hopfenberg (1978) described diffusion as both contributed by diffusion and polymer relaxation. They derived a model from Fick’s second law of diffusion by simple linear superposition. The diffusion component was derived from the sorption of particles at constant radius R and is dependent on the diffusion coefficient D . Equation 1 was further converted to make the boundaries homogeneous. Figure 4 shows the sequential diffusion-relaxation mechanism of hydrogel swelling.

Figure 5 shows the corresponding initial and boundary conditions for the diffusion component of the Berens-Hopfenberg model which can then be solved analytically via the Sturm-Liouville theory.

- initial condition (IC): initially within the hydrogel, the mass concentration p is equal to the radial position r multiplied by ρ_l which is the density at the hydrogel boundary
- first boundary condition (BC1): at the center of the hydrogel, the mass concentration p is zero
- second boundary condition (BC2): at the hydrogel boundary, the mass concentration p is zero

The relaxation component was assumed that the rate of the limiting relaxation step is first order with respect to the concentration difference where k_R is the relaxation rate constant. The Berens-Hopfenberg model, shown in Equation 3, accounts for the relative amount of particle uptake from diffusion and relaxation through the fractions x_F and x_R , respectively, which should add up to 1.

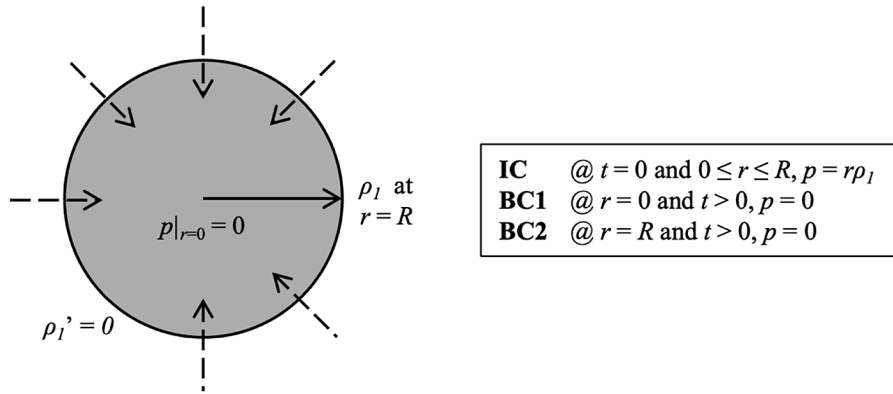


Figure 5. Diffusion component of the Berens-Hopfenberg model

$$\frac{M_t}{M_\infty} = x_F \left\{ 1 - \frac{6}{\pi^2} \sum_{n=0}^{\infty} \frac{1}{n^2} \exp \left[-D \left(\frac{n\pi}{R} \right)^2 t \right] \right\} + x_R [1 - \exp(-k_R t)] \quad (3)$$

where: x_F – uptake fraction through diffusion, x_R – uptake fraction through relaxation, R – radius of hydrogel.

Elaboudi et al. (2020) used the Berens-Hopfenberg model to characterize the sorption kinetics of poly-tetrafluoroethylene in different liquids. Through the model, they were able to prove that the contribution of polymer relaxation is more significant than the diffusion. This model is sometimes modified depending on the system and application. In glass fiber reinforced composites or GFRPs, da Silva et al. (2024) modified the model to account for post-curing effects on moisture absorption in epoxy matrix composites while Jiang et al. (2012) modified the model to account for the hydrolysis phenomenon by adding a third term.

Model for system with moving boundary

Both the Korsmeyer-Peppas model and Berens-Hopfenberg model do not account for the change in hydrogel size during swelling, as shown in Figure 6. Fick’s second law of diffusion may be used to derive a model for the diffusion of particles from in between phases wherein the boundary is moving. Crank (1979) obtained the concentration profiles for phases 1 and 2. These are initially derived for infinite media but were later proven to be applicable to media bounded by one or two planes.

Transport systems involving moving boundaries are often called a Stefan problem which was first demonstrated as the melting of a semi-infinite sheet of ice (Karabeni, 2016). Astaluta and Sarti (1978) provided experimental evidence of solvent penetration into glass polymers. This list of

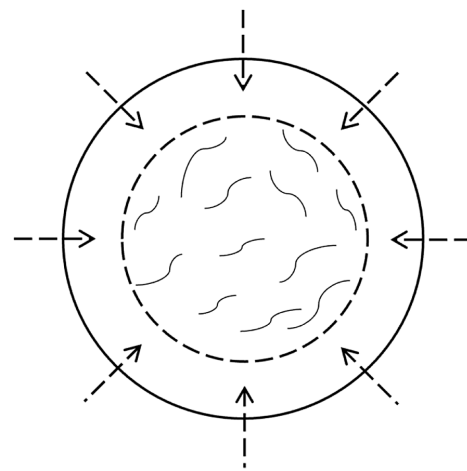


Figure 6. Swelling with moving boundary

evidence, summarized by Hsieh (2012), include the presence of a morphological discontinuity in the polymer that divides the glassy and rubbery regions. This interface moves at a rate which is initially constant.

With the complex solutions to problems involving systems with moving boundaries, several studies have developed a method in modeling these types of systems. One of the computational methods used by Gulkac (2010) to solve a two-dimensional fusion problem with convective boundary conditions was the locally one-dimensional (LOD) scheme which is an improvement of the typical finite difference methods. Karabeni (2016) used different numerical methods to address the complexities of a Stefan problem. These include variable space grid method, boundary immobilization method, and isotherm migration method to simplify the complex boundary conditions of the Stefan problem. Then, they utilized the cubic B-splines collocation finite element method to model the

simplified problem. These studies establish the usefulness of the methodology of Crank (1979) in developing models for diffusion with moving boundary for different geometries and applications, like for agricultural hydrogels with spherical geometries.

MATERIALS AND METHODS

Data gathering

Water sorption data from the reusability characterization test and nutrient release data of Andes et al. (2021) were retrieved. These available data were transformed into the fractional form M_t/M_∞ which may be used for data fitting and model validation. Masses of the swollen hydrogel through time were processed through Equation 4 (Garduque et al., 2020). Data for conductivity tests of the nutrient release in the bulk water medium was transformed through Equation 5.

$$\frac{M_t}{M_\infty} = \frac{m_t - m_{dry}}{m_{sat'd} - m_{dry}} \quad (4)$$

where: m_t – mass of the swollen hydrogel at any given time t , m_{dry} – mass of the dried hydrogel at $t = 0$, $m_{sat'd}$ is the mass at saturation.

$$\frac{M_t}{M_\infty} = \frac{X_t - X_i}{X_{sat'd} - X_i} \quad (5)$$

where: X_t – conductivity at any given time t , X_i – conductivity at $t = 0$, and $X_{sat'd}$ – conductivity at saturation.

Data fitting and model validation

The fractional mass ratio data M_t/M_∞ of first-cycle water sorption and nutrient release of Andes et al. (2021) were fitted into different models. The kinetic parameters determined from the first-cycle water sorption data fitting were validated using the second-cycle water sorption data of Andes et al. (2021).

Korsmeyer-Peppas model

The processed data for the first-cycle water sorption and nutrient release of Andes et al. (2021) were fitted into the Korsmeyer-Peppas model shown in Eq. 2 as performance reference of the succeeding models. The diffusion constant k and diffusion exponent n for the best-fit line were determined.

Berens-Hopfenberg model

The constant-radius sorption of a diffusion with relaxation is investigated. The processed data were fitted into the Berens-Hopfenberg model that characterizes the behavior of this mechanism, as shown in Equation 3. The fractions x_F and x_R , relaxation rate constant k_R , and D_0 were determined.

The Berens-Hopfenberg model assumes that the diffusion coefficient is constant. However, diffusion coefficient can be affected by system properties like concentration. A model for the concentration-dependence of the diffusion constant uses C as the solute concentration and β as the concentration coefficient (Amsden, 1998). This was incorporated into the modified Berens-Hopfenberg model to perform another data fitting as shown in Eq. 6. The diffusion coefficient at infinite dilution D_0 and concentration coefficient β were also determined aside from x_F , x_R , and k_R .

$$\frac{M_t}{M_\infty} = x_F \left\{ 1 - \frac{6}{\pi^2} \sum_{n=0}^{\infty} \frac{1}{n^2} \exp \left[-D_0 \exp(\beta C) \left(\frac{n\pi}{R} \right)^2 t \right] \right\} + x_R [1 - \exp(-k_R t)] \quad (6)$$

where: D_0 – diffusion coefficient at infinite dilution, β – concentration coefficient, C – solute concentration.

Model for diffusion with moving boundary

The variable-radius diffusion mechanism was investigated. As shown in Figure 7, the hydrogel initially has a radius of R_0 at time $t = 0$. Through time, the boundary $r = R$ between the hydrogel and bulk water phases moves along the positive radial direction as water molecules continue to diffuse into the hydrogel. Figure 7 also shows the corresponding initial and boundary conditions applied to the Fick's second law of diffusion in Equation 1 for both the hydrogel and bulk water phases. A series of combination of variables, integration by parts, and Laplace transforms was utilized to solve the differential equation. For the hydrogel phase A:

- initial condition (IC): initially within the hydrogel, the mass concentration in the hydrogel phase p_A is equal to the radial position r multiplied by C_i which is the initial concentration of the penetrant in the hydrogel phase
- first boundary condition (BC1): at the hydrogel boundary, the mass concentration in the hydrogel phase p_A approaches that of the initial condition
- second boundary condition (BC2): far outside the hydrogel boundary, the mass concentration in the hydrogel phase p_A is arbitrarily set to be equal to a constant a

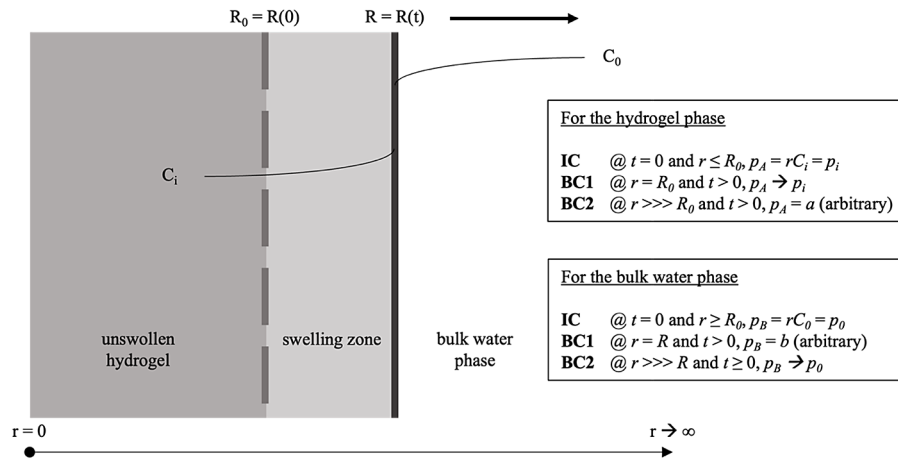


Figure 7. Phases in a swelling mechanism with moving boundary

For the bulk water phase B:

- initial condition (IC): initially outside the hydrogel, the mass concentration in the bulk water phase p_B is equal to the radial position r multiplied by C_0 which is the bulk concentration of the penetrant in the bulk water phase
- first boundary condition (BC1): at the hydrogel boundary, the mass concentration in the bulk water phase p_B is arbitrarily set to be equal to a constant b
- second boundary condition (BC2): far outside the hydrogel boundary, the mass concentration in the bulk water phase p_B approaches that of the initial condition
- The processed data were fitted into a semi-empirical model that represents this behavior.

A concentration profile was developed from Fick’s second law of diffusion. This concentration profile was simplified and converted into the fractional mass ratio M_t/M_∞ by imposing the following assumptions:

- constant temperature;

- diffusion is unidirectional because the edge effects are negligible;
- negligible external mass transfer resistance since the hydrogels are hydrophilic so the water molecules will not experience any resistances traveling to the hydrogel surface; and
- equal penetrant concentrations of the two phases at the boundary due to conditions of phase equilibria.

Coefficients were used to represent these assumptions to develop a semi-empirical model. The fractional mass ratio data were fitted into this model and the empirical coefficients along with the diffusion coefficient D were determined.

RESULTS AND DISCUSSION

Korsmeyer-Peppas model

As performance reference, the water sorption data and nutrient release data were first fitted

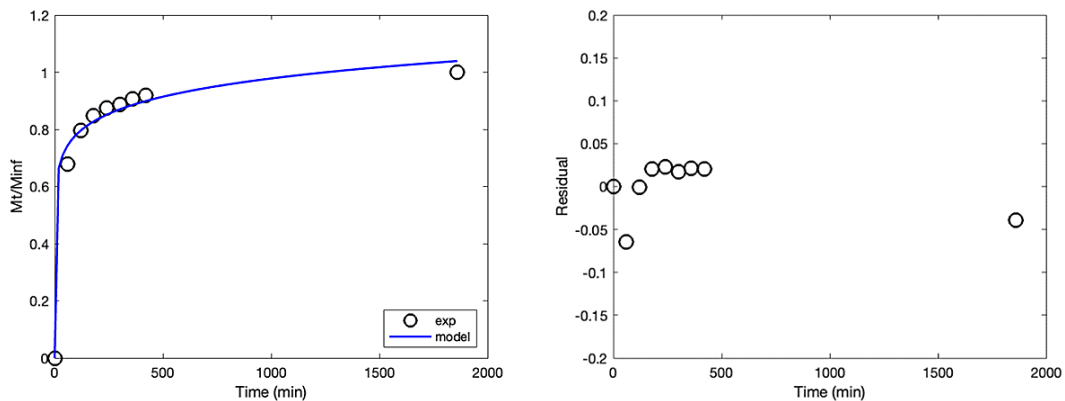


Figure 8. Korsmeyer-Peppas model for water sorption: (a) fitting, (b) residual plot

using the simple and commonly used Korsmeyer-Peppas model in Equation 2. Upon curve fitting of the data, kinetic parameters k and n were determined. Figure 8 shows the best-fit line and the corresponding residual plot of the water sorption data, and Figure 9 for the nutrient release data. Table 2 shows a summary of the kinetic parameters of the model.

As shown in Table 2 and referring Table 1, both water sorption and nutrient release behavior have n values below 0.5, depicting a pseudo Fickian diffusion. This could mean that the data sets do not fit well with the model, as also shown by the low values of R^2 . The poor data fitting, as shown by the low values of R^2 , can also be verified by the distribution of residuals. The model must be able to predict the response that only the inherent randomness contributes to the error portion of the observed value. Ideally, the model is a good approximation to the data set if the residuals are randomly scattered around the x-axis. However, Figures 8b and 9b follow a non-random pattern, evident from the initial steep rise followed by a gradual fall. This pattern indicates that the deterministic portion (time-variable) of the model is not able to capture some explanatory information that may have also affected the residuals (Everitt and Skrondal, 2010). When subjected to the Shapiro-Wilk test for normality at an alpha value of 0.05, both data sets of residuals failed.

A limitation of the Korsmeyer-Peppas model is that it fits accurately only the first 60% of accumulated uptake or release (Ritger and Peppas, 1987). The first 60% of the nutrient release data can be selectively fitted to the Korsmeyer-Peppas model. The best-fit line is shown in Figure 9 with a high agreement of $R^2 = 0.9993$. The calculated parameters for the first 60% is $k = 0.2854$ and $n =$

0.5610 which are significantly different from the values reported in Table 2. In this truncated data set, a realistic value of n was obtained, depicting an anomalous non-Fickian diffusion wherein the rates of diffusion and of relaxation are comparable to each other (Korsmeyer et al., 1983). These comparable rates are manifested as hydrogels transition from a partially rubbery to glassy state (Ganji et al., 2010).

Berens-Hopfenberg model

Swelling kinetics that follow Fick's laws of diffusion is unlikely to prevail throughout the entire swelling phenomenon, especially if diffusion is no longer controlling and is instead replaced by stress relaxation. Relaxation exists in polymer matrices when interchain hydrogen bonds rupture at an increasing number of sites (Schott, 1992).

An accurate model for the diffusion-relaxation mechanism of the sorption of solute is the Berens-Hopfenberg model shown in Equation 3 which is a superposition of the Fickian diffusion and first-order relaxation. This model is conceptualized through the idea of constant-size sorption. The Berens-Hopfenberg model used in the curve fitting of the water sorption data and nutrient release data is presented in Eq. 7. Figure 10 shows the best-fit line and the corresponding

Table 2. Kinetic parameters of the Korsmeyer-Peppas model

Kinetic parameter	Water sorption	Nutrient release
Diffusion constant, k	0.4993	0.4747
Diffusion exponent, n	0.0974	0.2208
R^2	0.9893	0.9130

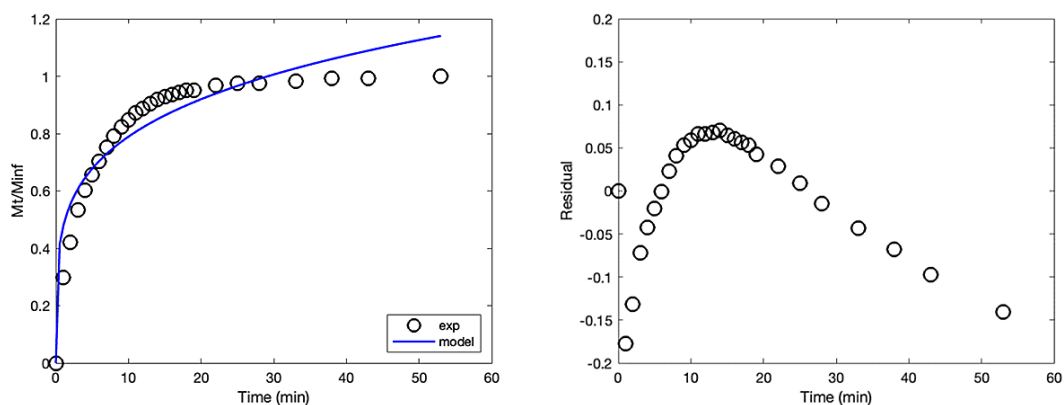


Figure 9. Korsmeyer-Peppas model for nutrient release: (a) fitting, (b) residual plot

residual plot of the water sorption data, and Figure 11 for the nutrient release data. Table 3 shows a summary of the obtained kinetic parameters of the Berens-Hopfenberg model in Equation 7.

$$\frac{M_t}{M_\infty} = x_F \left\{ 1 - \frac{6}{\pi^2} \sum_{n=0}^{\infty} \frac{1}{n^2} \exp[-D'(n\pi)^2 t] \right\} + x_R [1 - \exp(-k_R t)] \quad (7)$$

where: D' – lumped coefficient for D and R .

Figures 10b and 11b follow a random pattern, indicating a good representation of the Berens-Hopfenberg model (Everitt and Skrondal, 2010). As shown in Table 3, both behaviors had significant values of x_R than x_F . This confirms that there is sorption through diffusion and relaxation. A two-stage sorption process is present where the initial stage is when solutes diffuse into a polymer matrix followed by a stage where polymer chains relax (Thybring et al., 2019). Specifically, x_R values for both water sorption and nutrient release are greater than x_F depicting greater water uptake during relaxation than diffusion. Stress relaxation during swelling can be divided further into two

stages: first wherein the stresses of hydrogels decrease rapidly with time, followed by a gradual decrease wherein the relaxation basically reaches equilibrium (Sun et al., 2021).

The k_R values are greater than the lumped coefficient D' for both behaviors. This means that the sorption process of the hydrogels is relaxation-controlled (Zang et al., 2019). The rearrangement of the polymer chains due to the penetrants increases the available free volume for more penetrants to diffuse (Wind and Lenderink, 1995). For cellulose-based swellable polymers like the

Table 3. Kinetic parameters of the Berens-Hopfenberg model

Kinetic parameter	Water sorption	Nutrient release
Diffusion fraction, x_f	0.3786	0.4940
Relaxation fraction, x_r	0.6214	0.5060
Lumped diffusion coefficient, D' (min^{-1})	0.0002595	0.02726
Relaxation rate constant, k_r (min^{-1})	0.03308	0.1332
R^2	0.9999	0.9995

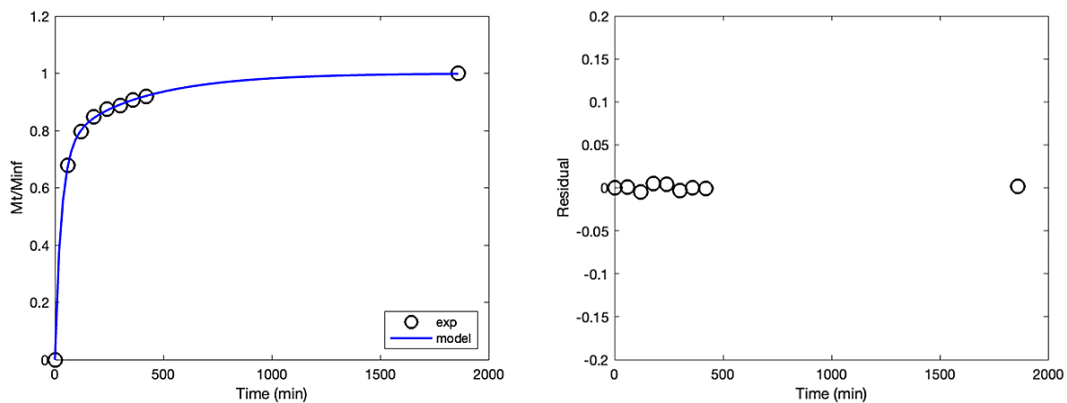


Figure 10. Berens-Hopfenberg model for water sorption: (a) fitting, (b) residual plot

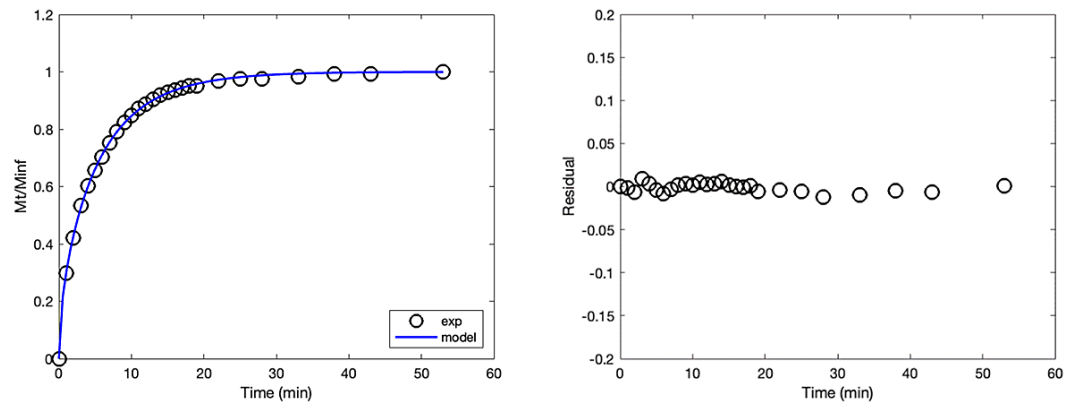


Figure 11. Berens-Hopfenberg model for nutrient release: (a) fitting, (b) residual plot

HPC/CMC/Alg hydrogel matrix, stress relaxation dominates due to faster diffusion rates at high moisture content (Thybring et al., 2019). The hydrogen bonding from the hydroxyl groups present in the cellulose derivatives easily responds to the swelling stress induced by osmotic pressure (Hopfenberget al., 1976). As for nutrient release, hydrogels assume a compact structure wherein nutrient release could take place significantly if the polymeric chains relax (Tan et al., 2008).

The dependence of the diffusion coefficient on concentration was investigated through the modified Berens-Hopfenberg equation. Following the similar modification in lumping D and R , the concentration-dependent Berens-Hopfenberg model in Equation 6 is further modified to Equation 8 where water sorption data and nutrient release data are subjected into fitting. Figure 12 shows the best-fit line and the corresponding residual plot of the water sorption data, and Figure 13 for the nutrient release data. Table 4 shows a summary of the kinetic parameters of the model in Equation 8.

$$\frac{M_t}{M_\infty} = x_F \left\{ 1 - \frac{6}{\pi^2} \sum_{n=0}^{\infty} \frac{1}{n^2} \exp[-D_0' \exp(\beta C) (n\pi)^2 t] \right\} + x_R [1 - \exp(-k_R t)] \quad (8)$$

where: D_0' – lumped coefficient for D_0 and R .

Figures 12b and 13b follow a random pattern, indicating a good representation of this modified Berens-Hopfenberg model for the data sets (Everitt and Skronchal, 2010). The values in Table 4 did not vary significantly from those in Table 3. Even in this modified Berens-Hopfenberg model, polymer relaxation is more pronounced than diffusion in the sorption of this cellulose-based hydrogel.

From Table 4, the nutrient release behavior obtained a higher value of β . The dependence of the diffusion coefficients on concentration cannot be modeled easily and there is no single predictive correlation that can provide a good estimate (Poling et al., 2001). Nevertheless, a common understanding about this correlation is that the diffusion coefficients increase with concentration. This can be supported by the simple analogy that the amount of solutes in bulk are directly

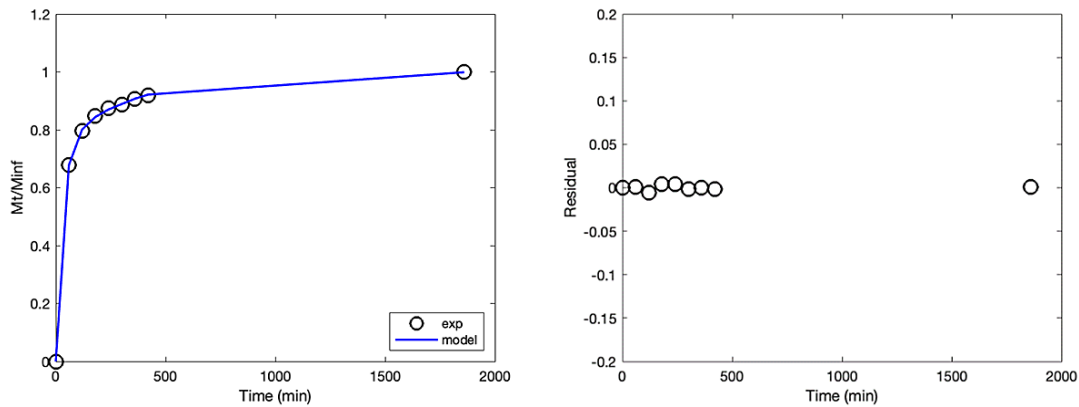


Figure 12. Modified Berens-Hopfenberg model for water sorption: (a) fitting, (b) residual plot

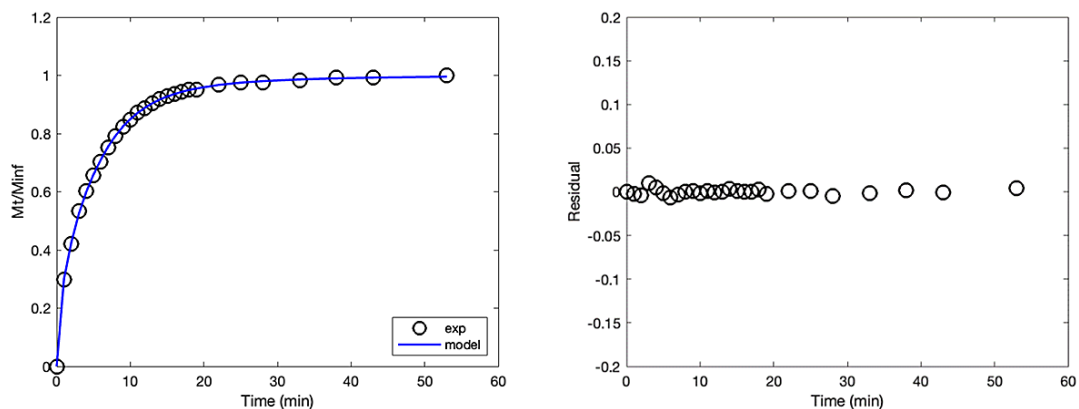


Figure 13. Modified Berens-Hopfenberg model for nutrient release: (a) fitting, (b) residual plot

proportional to the amount of solutes that can transport through a certain plane or membrane.

Semi-empirical model for diffusion with moving boundary

Since the hydrogel surface represents one of the mass transfer boundaries, its movement represents a dynamic behavior of the diffusion path length. A specific model by Crank (1979) can be derived from Fick’s second law of diffusion for the schematic illustration in Figure 7. The concentration profile of a penetrant diffusing into phase A from B can be represented by the derived Equations 9 and 10 (Crank, 1979).

$$\frac{C_A - C_i}{C_A|_R - C_i} = \operatorname{erfc}\left(\frac{r - R}{\sqrt{4D_A t}}\right) \quad (9)$$

$$\frac{C_0 - C_B}{C_0 - C_B|_R} = \operatorname{erfc}\left(\frac{r - R}{\sqrt{4D_B t}}\right) \quad (10)$$

where: C – concentration of the penetrant in phases A and B at any radial position r and time t , $C|_R$ – concentration at the hydrogel boundary, R – radial position of the boundary, D – diffusion coefficient of the penetrant in phases A and B, C_i – initial concentration of the penetrant in phase A, C_0 – bulk concentration of the penetrant in phase B.

The rate at which the boundary is moving can be derived from these two profiles. This can be simplified into Equation 11 where K is a lumped coefficient on D_A, D_B, C_0 , and C_i .

$$R(t) = R_0 + K\sqrt{t} \quad (11)$$

where: R – radius of hydrogel at any time t , R_0 – initial radius of hydrogel, K – lumped coefficient for D_A, D_B, C_0 , and C_i .

Table 4. Kinetic parameters of the modified Berens-Hopfenberg model

Kinetic parameter	Water sorption	Nutrient release
Diffusion fraction, x_f	0.3083	0.2398
Relaxation fraction, x_r	0.6917	0.7602
Relaxation rate constant, k_r (min ⁻¹)	0.03452	0.1613
Lumped diffusion coefficient, D_0' (min ⁻¹)	0.00000964	0.05976
Concentration coefficient, β	0.1641	0.9205
R^2	0.9999	0.9992

The following steps detail the derivation of the semi-empirical model developed in this study:

- Assuming negligible external mass transfer resistance, the system will only consider Eq. 9 in modeling where mass transfer resistance in the hydrogel phase A is significant.
- In converting the fractional concentration ratios to fractional mass ratios M_t/M_∞ , a correction factor A is introduced as a coefficient of the complementary error function.
- The swelling length in the argument of the complementary error function is represented instead by the swelling radius determined through Equation 11 since radial position does not affect the total mass uptake at any given time t .

The developed semi-empirical model, shown in Equation 12, was used to fit the data for water sorption and nutrient release. Figure 14 shows the best-fit line and the corresponding residual plot of the water sorption data, and Figure 15 for the nutrient release data. Table 5 shows a summary of the kinetic parameters of the semi-empirical model in Equation 12.

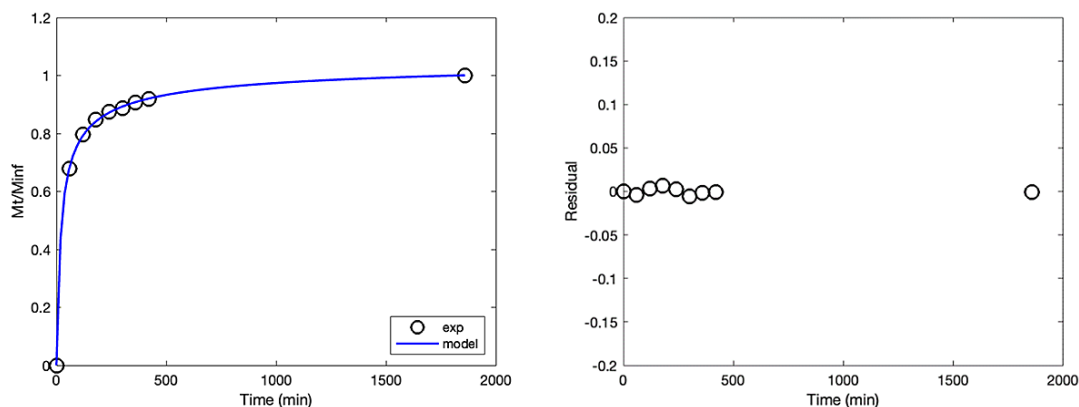


Figure 14. Semi-empirical model for water sorption: (a) fitting, (b) residual plot

$$\frac{M_t}{M_\infty} = A \operatorname{erfc}\left(\frac{R}{\sqrt{4Dt}}\right) \quad (12)$$

where: A – correction factor, R – radius of hydrogel at any time t , D – diffusion coefficient.

Figure 14b follows a random pattern while that in Figure 15b does not. Moreover, when subjected to the Shapiro-Wilk test for normality at an alpha value of 0.05, the residuals data set for nutrient release failed. Swelling experiments should take note of the hydrogel size at different time intervals to improve precision of residual data. Moreover, models can be better fitted with concentration vs. time data, so it would be better if actual concentrations are measured (e.g., via spectroscopy) instead of masses from gravimetric methods. This can also improve accuracy of the R^2 values in Table 5 which may have been affected by the assumptions made to arrive at Equation 12. The lumped coefficient K was determined via Eq. 11 using the final hydrogel size and saturation time. As shown in Table 5, the nutrient release had a larger K than in water sorption because the nutrient release took a much shorter time by about 55 minutes to achieve saturation than water sorption by about 1800 minutes.

The correction factor A is an empirical coefficient that accounts for the possible deviations of the conversion of concentration ratios to mass ratios. It should be equal to 1 if it were an ideal conversion. However, the obtained values are greater than 1 as shown in Table 5. This may be attributed to the possible change in density of the hydrogel bead through time since its mass and volume also change accordingly. This erratic behavior can also be attributed to the nature of the hydrogel. Natural hydrogels such as cellulose-based hydrogels are highly biocompatible and bioavailable leading to a high batch-to-batch variation (Catoira et

Table 5. Kinetic parameters of the semi-empirical model

Kinetic parameter	Water sorption	Nutrient release
Lumped coefficient, K	0.03425	0.2029
Correction factor, A	1.2170	1.5937
Diffusion coefficient, D (mm ² /min)	0.02723	0.2479
R^2	0.9998	0.9887

al., 2019). Despite being advantageous on actual agricultural applications, this high unpredictability and low reproducibility of data on natural hydrogels is a disadvantage (Radaza et al., 2022).

Across all models, the diffusion coefficients (D or D') are larger in the nutrient release behavior than in water sorption. This means that the diffusion path length of the nutrients is larger than that of water molecules. This can be attributed to the relatively larger sizes of fertilizer solutes like nitrogen, phosphorus, and potassium.

Model validation

The second-cycle water sorption data of Andes et al. (2021) was converted to M_t/M_∞ through Equation 4. As shown in Figure 16, this was plotted against the predicted values when using the determined parameters from the modified Berens-Hopfenberg model and the semi-empirical model. Ideally, a good agreement of the data and the predictive model can be concluded if the points lie at or around the diagonal line since y_{actual} is equal to or around the value of $y_{predicted}$. Most values in Figure 16 are overestimated, i.e., lie below the diagonal line. There are huge discrepancies from the diagonal line at smaller values of

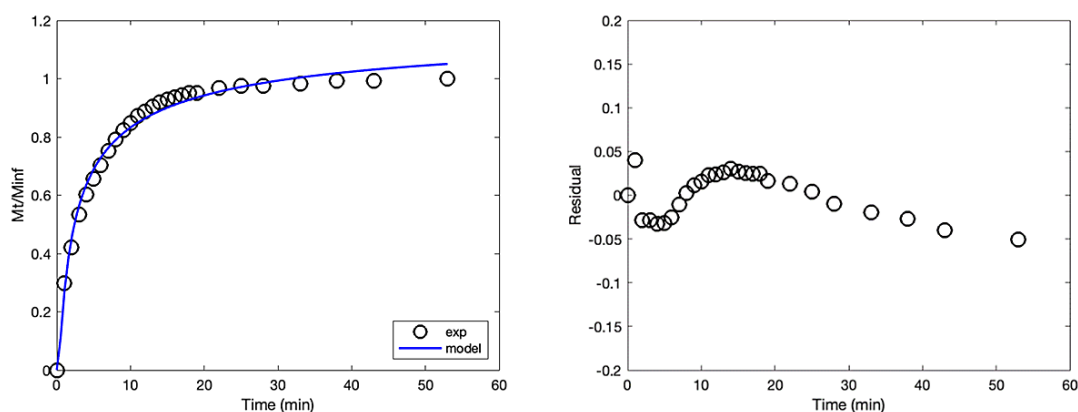


Figure 15. Semi-empirical model for nutrient release: (a) fitting, (b) residual plot

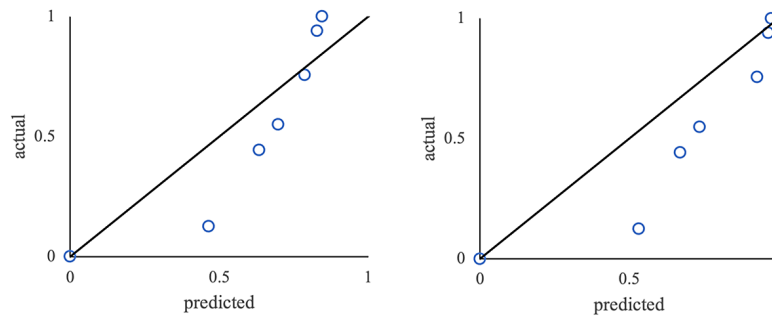


Figure 16. Water sorption data validated with the parameters from: (a) modified Berens-Hopfenberg model, (b) semi-empirical model

Table 6. Comparison of obtained parameters for first-cycle and second-cycle water sorption

Model	Kinetic parameter	First cycle	Second cycle
Modified Berens-hopfenberg model	Diffusion fraction, x_r	0.3086	0.5656
	Relaxation fraction, x_r	0.6914	0.4344
	Relaxation rate constant, k_r (min^{-1})	0.03452	0.01829
	Lumped diffusion coefficient, D_0' (min^{-1})	0.00000981	0.00002501
	Concentration coefficient, β	0.1632	0.4356
Semi-empirical model for diffusion w/ moving boundary	Lumped coefficient, K	0.03425	0.03814
	Correction factor, A	1.2170	1.4947
	Diffusion coefficient, D (mm^2/min)	0.02723	0.007646

M_t/M_∞ , implying a significant extent of variation in the diffusion stages which happens at the initial periods of water sorption. By computing the root mean squares error (RMSE) of the two data sets, the Korsmeyer-Peppas model provided the fit with least agreement (RMSE = 0.2284) while the concentration-dependent Berens-Hopfenberg model provided the best (RMSE = 0.1701). This can be attributed to the use of fewer assumptions to model the behavior unlike the semi-empirical model for diffusion with moving boundary.

To compare the actual kinetic parameters of the two data sets, the second-cycle water sorption data were fitted into the concentration-dependent Berens-Hopfenberg model and the semi-empirical model for diffusion with moving boundary. The determined parameters are shown in Table 6. For the modified Berens-Hopfenberg model, the second cycle has a moisture uptake greater in diffusion than in relaxation, as shown by the $x_F > x_R$. Moreover, despite the decrease in D_0' , the β is much larger in the second cycle which means the concentration-dependence of the diffusion coefficient is more pronounced. For the semi-empirical model, the slight change in K is affected by the difference in saturation times for the two water sorption cycles. The diffusion coefficient also

decreased, like the modified Berens-Hopfenberg model. The maximum water absorption capacity decreases as the number of cycles progress (Andes et al., 2021). The hydrogel matrix undergoes a rearrangement during the deswelling process so it can accommodate sorption in the next swelling cycle (Enscore et al., 1980). Moreover, the initial mass of the hydrogel in the second cycle is lower than that in the first cycle and will continue to decrease after more cycles of swelling-deswelling. This lower initial mass causes a lower capacity of accommodating water molecules due to the physical changes upon deswelling, leading to an increase in hydrogel rigidity. As for other mechanical properties of hydrogels, there is a significant reduction in the stretchability of crosslinked hydrogels, whether its swelling-deswelling or deswelling-swelling. The rupture of short chains results in the failure of the entire hydrogel network (Huang and Liu, 2024).

CONCLUSIONS

The increasing interest in hydrogel technology for agricultural applications has resulted in several recent studies on performance tests of

different types of hydrogels. Existing kinetic modelling studies rely mostly on the commonly used Korsmeyer-Peppas model and the Berens-Hopfenberg model, which are too ideal and often yield inaccurate parameters.

In this study, data on water sorption and nutrient release were subjected to data fitting into several models of mass transport. For both data sets, the Korsmeyer-Peppas model yielded a pseudo Fickian type of transport, which is unrealistic as the model is only accurate for the first 60% of diffusion. Moreover, the concentration-dependence of the diffusion coefficient provided a better fit to the previous Berens-Hopfenberg model, which assumed that the diffusion coefficient as constant. To account for the real-time change in hydrogel size during swelling, a semi-empirical model was developed through several assumptions. This model also yielded a more accurate fit compared to the Korsmeyer-Peppas and Berens-Hopfenberg models.

The obtained kinetic parameters can be used in simulating the effectivity of the use of bio-based hydrogels in agriculture as (i) water carriers in times of water shortage and (ii) nutrient carriers to address fertilizer underutilization. The study revealed that the relaxation process of hydrogels contributes to sorption more than the diffusion process. Moreover, the study was able to derive novel and more accurate models in mass transport that account for non-idealities that have never been considered before in kinetic studies particular to agricultural applications. This opens possibilities of further research where modelling of mass transport in hydrogels can be more precise by developing system-specific models. This can also benefit mass transport applications in other fields such as pharmaceutical, biomedical, and environmental.

Acknowledgments

The authors acknowledge the Office of the Chancellor of the University of the Philippines Diliman, through the Office of the Vice Chancellor for Research and Development, for funding support through the Outright Research Grant.

REFERENCES

1. Akalin, G. O., & Pulat, M. (2018). Preparation and characterization of nanoporous sodium carboxymethyl cellulose hydrogel beads.

- Journal of Nanomaterials*, 2018, 1–12. <https://doi.org/10.1155/2018/9676949>
2. Amsden, B. (1998). Solute Diffusion within hydrogels. Mechanisms and models. *Macromolecules*, 31(23), 8382–8395. <https://doi.org/10.1021/ma980765f>
3. Andes, J. F. E., Jao, A. F., Zacarias, J. H., & Tumolva, T. (2021). Performance testing of NaCMC/HPC/NaAlg hydrogels for agricultural applications. *Key Engineering Materials*, 891, 105–110. <https://doi.org/10.4028/www.scientific.net/KEM.891.105>
4. Astaluta, G., & Sarti, G. C. (1978). A class of mathematical models for sorption of swelling solvents in glassy polymers. *Polymer Engineering & Science*, 18(5), 388–395. <https://doi.org/10.1002/pen.760180510>
5. Berens, A. R., & Hopfenberg, H. B. (1978). Diffusion and relaxation in glassy polymer powders: 2. Separation of diffusion and relaxation parameters. *Polymer*, 19(5), 489–496. [https://doi.org/10.1016/0032-3861\(78\)90269-0](https://doi.org/10.1016/0032-3861(78)90269-0)
6. Boztepe, C., Solener, M., Yuceer, M., Kunkul, A., & Kabasakal, O. S. (2015). Modeling of swelling behaviors of acrylamide-based polymeric hydrogels by intelligent system. *Journal of Dispersion Science and Technology*, 36(11), 1647–1656. <https://doi.org/10.1080/01932691.2014.996892>
7. Casalme, L. A., Nalzaro, P. J., Osabel, R. J., & Tumolva, T. (2016). *Microencapsulation of α -tocopherol using hydroxypropyl cellulose-blended sodium alginate*. University of the Philippines.
8. Catoira, M. C., Fusaro, L., Di Francesco, D., Ramella, M., & Boccafocchi, F. (2019). Overview of natural hydrogels for regenerative medicine applications. *Journal of Materials Science. Materials in Medicine*, 30(10), 115. <https://doi.org/10.1007/s10856-019-6318-7>
9. Chiarelli, P., De Rossi, D., & Basser, P. (1993). Hydrogel stress-relaxation. *Journal of Intelligent Material Systems and Structures*, 4(2), 176–183. <https://doi.org/10.1177/1045389X9300400206>
10. Crank, J. (1979). *The Mathematics of Diffusion* (2nd ed.). Oxford University Press.
11. da Silva, G. de A. S., d’Almeida, J. R. M., & Cardoso, D. C. T. (2024). Investigation on moisture absorption behavior on GFRP and neat epoxy systems in hygrothermal salt fog aging. *Composites Part B: Engineering*, 272, 111214. <https://doi.org/10.1016/j.compositesb.2024.111214>
12. Elaboudi, I., Mdarhri, A., Brosseau, C., Nourdine, A., Rzaizi, M., & Servant, L. (2020). Comparing the sorption kinetics of poly-tetrafluoroethylene processed either by extrusion or spark plasma sintering. *Polymer*, 190, 122192. <https://doi.org/10.1016/j.polymer.2020.122192>

13. Ensore, D. J., Hopfenberg, H. B., & Stannett, V. T. (1980). Diffusion, swelling, and consolidation in glassy polystyrene microspheres. *Polymer Engineering & Science*, 20(1), 102–107. <https://doi.org/10.1002/pen.760200117>
14. Everitt, B. S., & Skronal, A. (2010). *The Cambridge Dictionary of Statistics* (4th ed.). Cambridge University Press.
15. Fei, J., Tang, T., Zhou, L., He, H., Ma, M., Shi, Y., Chen, S., & Wang, X. (2024). Swelling behavior of sodium lignosulfonate grafted polyacrylic acid highly absorbent hydrogels with two-phase structure. *Polymer*, 300, 126828. <https://doi.org/10.1016/j.polymer.2024.126828>
16. Fosca, M., Rau, J. V., & Uskoković, V. (2022). Factors influencing the drug release from calcium phosphate cements. *Bioactive Materials*, 7, 341–363. <https://doi.org/10.1016/j.bioactmat.2021.05.032>
17. Ganji, F., Vasheghani-Farahani, S., & Vasheghani-Farahani, E. (2010). Theoretical description of hydrogel swelling: A review. *Iranian Polymer Journal*, 19(5).
18. Garduque, R. G., Gococo, B. J., Yu, C. A., Nalzar, P. J., & Tumolva, T. (2020). Synthesis and characterization of sodium carboxymethyl cellulose/sodium alginate/hydroxypropyl cellulose hydrogel for agricultural water storage and controlled nutrient release. *Solid State Phenomena*, 304, 51–57. <https://doi.org/10.4028/www.scientific.net/SSP.304.51>
19. Giustiniani, A., Ilyas, M., Indei, T., & Gong, J. P. (2023). Relaxation mechanisms in hydrogels with uniaxially oriented lamellar bilayers. *Polymer*, 267, 125686. <https://doi.org/10.1016/j.polymer.2023.125686>
20. Hsieh, M. H.-N. (2012). *Mathematical modelling of controlled drug release from polymer microspheres: Incorporating the effects of swelling, diffusion and dissolution via moving boundary problems*. Queensland University of Technology.
21. Huang, R., & Liu, Z. (2024). The effect of swelling/deswelling cycles on the mechanical behaviors of the polyacrylamide hydrogels. *Polymer*, 312, 127634. <https://doi.org/10.1016/j.polymer.2024.127634>
22. Jiang, X., Kolstein, H., & Bijlaard, F. S. K. (2012). Moisture diffusion and hygrothermal aging in pultruded fibre reinforced polymer composites of bridge decks. *Materials & Design*, 37, 304–312. <https://doi.org/10.1016/j.matdes.2012.01.017>
23. Karabenli, H. (2016). Numerical solutions for a Stefan problem. *New Trends in Mathematical Science*, 4(4), 175–175. <https://doi.org/10.20852/ntmsci.2016422668>
24. Korsmeyer, R. W., Gurny, R., Doelker, E., Buri, P., & Peppas, N. A. (1983). Mechanisms of solute release from porous hydrophilic polymers. *International Journal of Pharmaceutics*, 15(1), 25–35. [https://doi.org/10.1016/0378-5173\(83\)90064-9](https://doi.org/10.1016/0378-5173(83)90064-9)
25. Lin, J., Li, J., Gong, W., Liu, Y., Ai, Y., He, A., & Nie, H. (2024). A multi-responsive actuator with sensing capability based on poly (N-isopropyl acrylamide)/poly (sodium acrylate) Janus hydrogels. *Composite Structures*, 339, 118141. <https://doi.org/10.1016/j.compstruct.2024.118141>
26. Magcale-Macandog, D., Paraiso, P. M., Salvacion, A., Estadola, R., Quiñones, S. G., Silapan, I. M., & Briones, R. (2016). *An Overview of Agricultural Pollution in the Philippines: The Crops Sector*. World Bank. www.worldbank.org
27. Nalzar, P. J. B., Doctor, J. N. P., Domingo, J. R. C., Madrid, L. L. B., & Tumolva, T. P. (2019). A Modelling Study on the Degradation of Hydroxypropyl Cellulose/Sodium Alginate Blend Microcapsules for Controlled Drug Delivery. *Basic & Clinical Pharmacology & Toxicology*, 124, 12–12.
28. Nguyen, D.-V., Yuan, Y., Kukumberg, M., Wang, L., Lim, S. H., Hassanbhai, A. M., Chong, M., Kofidis, T., Tan, E. C. K., Seliktar, D., Kang, L., & Rufaihah, A. J. (2024). Controlled release of vancomycin from PEGylated fibrinogen polyethylene glycol diacrylate hydrogel. *Biomaterials Advances*, 161, 213896. <https://doi.org/10.1016/j.bioadv.2024.213896>
29. Nicasy, R. J. K., Waldner, C., Erich, S. J. F., Adan, O. C. G., Hirn, U., & Huinink, H. P. (2024). Liquid uptake in porous cellulose sheets studied with UFI-NMR: Penetration, swelling and air displacement. *Carbohydrate Polymers*, 326, 121615. <https://doi.org/10.1016/j.carbpol.2023.121615>
30. Philippine Statistics Authority. (2024). *Q1 2022 to Q2 2024 National Accounts of the Philippines*. <https://psa.gov.ph/system/files/nap/Q2%2024%20NAP%20Publication.pdf>
31. Qureshi, M. A. U. R., Arshad, N., Rasool, A., Rizwan, M., & Rasheed, T. (2023). Guar gum-based stimuli responsive hydrogels for sustained release of diclofenac sodium. *International Journal of Biological Macromolecules*, 250, 126275. <https://doi.org/10.1016/j.ijbiomac.2023.126275>
32. Radaza, I. C., Rizada, J. F., Tan, M. J., Nalzar, P. J., & Tumolva, T. (2022). *Modeling of Swelling and pH-Dependent Nutrient Release Kinetics of HPC/CMC/Alginate Hydrogel Blends for Agricultural Applications*. <https://technoaretepublication.org/book/smart-environmental-science-technology-management/paper/6.pdf>
33. Ritger, P. L., & Peppas, N. A. (1987). A simple equation for description of solute release I. Fickian and non-fickian release from non-swelling devices in the form of slabs, spheres, cylinders or discs. *Journal of Controlled Release*, 5(1), 23–36. [https://doi.org/10.1016/0168-3659\(87\)90034-4](https://doi.org/10.1016/0168-3659(87)90034-4)
34. Rizwan, M., Naseem, S., Gilani, S. R., & Durrani, A. I. (2024). Optimization of swelling and mechanical behavior of Acer platanoides cellulose combo

- hydrogel. *Kuwait Journal of Science*, 51(2), 100177. <https://doi.org/10.1016/j.kjs.2024.100177>
35. Saruchi, Kumar, V., Mittal, H., & Alhassan, S. M. (2019). Biodegradable hydrogels of tragacanth gum polysaccharide to improve water retention capacity of soil and environment-friendly controlled release of agrochemicals. *International Journal of Biological Macromolecules*, 132, 1252–1261. <https://doi.org/10.1016/j.ijbiomac.2019.04.023>
36. Sun, W., Hu, Y., Cheng, Y., Yang, S., & Kang, Z. (2021). Effect of cross-linking methods on stress relaxation of PVA/PAM-co-PAA-based hydrogels. *International Journal of Polymer Analysis and Characterization*, 26(4), 330–341. <https://doi.org/10.1080/1023666X.2021.1889739>
37. Takigawa, T., Ikeda, T., Takakura, Y., & Masuda, T. (2002). Swelling and stress-relaxation of poly(N-isopropylacrylamide) gels in the collapsed state. *The Journal of Chemical Physics*, 117(15), 7306–7312. <https://doi.org/10.1063/1.1507103>
38. Thybring, E. E., Glass, S. V., & Zelinka, S. L. (2019). Kinetics of water vapor sorption in wood cell walls: state of the art and research needs. *Forests*, 10(8), 704. <https://doi.org/10.3390/f10080704>
39. Yang, B., Chen, X. D., & Mercadé-Prieto, R. (2021). Stress relaxation of particulate whey protein hydrogels. *Food Hydrocolloids*, 118, 106786. <https://doi.org/10.1016/j.foodhyd.2021.106786>
40. Yetilmezsoy, K., Kıyan, E., & İlhan, F. (2024). Synthesis of agro-industrial wastes/sodium alginate/bovine gelatin-based polysaccharide hydrogel beads: Characterization and application as controlled-release microencapsulated fertilizers. *International Journal of Biological Macromolecules*, 279, 135382. <https://doi.org/10.1016/j.ijbiomac.2024.135382>
41. Zang, J., Wang, K., & Liu, A. (2019). Phenomenological over-parameterization of the triple-fitting-parameter diffusion models in evaluation of gas diffusion in coal. *Processes*, 7(4), 241. <https://doi.org/10.3390/pr7040241>
42. Zhang, Q., Huang, Z., Jiang, H., Wu, M., Dong, Z., Chen, C., Chen, F., Zhao, G., & Ma, P. (2025). “Bamboo-like” strong and tough sodium alginate/polyacrylate hydrogel fiber with directional controlled release for wound healing promotion. *Carbohydrate Polymers*, 347, 122761. <https://doi.org/10.1016/j.carbpol.2024.122761>
43. Zhang, X., Zhang, H., Lv, X., Xie, T., Chen, J., Fang, D., & Yi, S. (2024). Construction of mechanically robust and recyclable catalytic hydrogel based on hydroxypropyl cellulose-supported by montmorillonite/ionic liquid with different anions for pollutants(4-NP, MB, CR, Rhb) degradation. *International Journal of Biological Macromolecules*, 273, 132788. <https://doi.org/10.1016/j.ijbiomac.2024.132788>